Surface & Coatings Technology 403 (2020) 126340

Contents lists available at ScienceDirect

Surface & Coatings Technology

journal homepage: www.elsevier.com/locate/surfcoat

Enhanced mechanical and corrosion protection properties of pulse electrodeposited NiP-ZrO_2 nanocomposite coatings

Mostafa H. Sliem[a,1], Khuram Shahzad[a,b,1], V.N. Sivaprasad[c], R.A. Shakoor[a,*], Aboubakr M. Abdullah[a,*], Osama Fayyaz[a], Ramazan Kahraman[c], Malik Adeel Umer[b,*]

[a] Center for Advanced Materials (CAM), Qatar University, 2713 Doha, Qatar
[b] Department of Materials Engineering, School of Chemical and Materials Engineering, National University of Science and Technology (NUST), Islamabad, Pakistan
[c] Departments of Chemical Engineering, College of Engineering, Qatar University, Doha, Qatar

ARTICLE INFO

Keywords:
Nanocomposite (NC) coatings
Pulse electrodeposition
Microhardness
Corrosion protection
Surface topography
Structural analysis

ABSTRACT

Pulse electrodeposition is a technique of particular interest, which offers promising advantages such as ease of processing, compositional control, uniformity in structure, and grain refinement. In the present study, NiP-ZrO_2 nanocomposite coatings containing various concentrations of ZrO_2 nanoparticles (ZONPs) were deposited on low alloy steel (30CrMnSi) through pulse electrodeposition technique. The ZONPs in concentration of 0.0, 0.25, 0.50, 0.75, and 1.0 g/L were added in the electrolyte bath to obtain NiP-ZrO_2 nanocomposite coatings. Furthermore, to elucidate the role of ZONPs in the NiP matrix, the structural, morphological, mechanical, and electrochemical properties of NiP-ZrO_2 nanocomposite coatings were studied thoroughly. FESEM and EDX results reveal the successful incorporation of ZONPs into the NiP matrix. XRD and XPS analysis confirm the formation of a pure phase NiP structure without any noticeable defects. A considerable improvement in the mechanical response was observed with an increasing amount of ZONPs, reaching to highest values (hardness 6.7 GPa, modulus of elasticity 21.72 GPa) for NiP-1.0 ZrO_2 coating composition. Similarly, the electrochemical results show a gradual increase in corrosion protection behavior of the NiP-ZrO_2 coatings with increasing ZONP concentration, reaching an eventual value ~5.8 $k\Omega\,cm^{-2}$ at NiP-1.0 ZrO_2 coating composition, which is six times greater than the pure NiP coatings. These improvements in the mechanical and electrochemical response of NiP-ZrO_2 nanocomposite coatings highlight their suitability for applications such as oil and gas pipelines.

1. Introduction

Material deterioration due to the interaction with environment can degrade the performance of components over time [1]. Corrosion, one of the leading causes of part failure, damages the surfaces of the materials, and sometimes combines with wear leads to accelerate deterioration process [2]. Thus, there is a dire need for the modification of the surface properties instead of improving the bulk material [3]. Optimal surface protection is particularly crucial for materials subjected to severe conditions, such as for aircraft and refineries [4]. Currently, inorganic coatings are gaining importance due to their cost-effectiveness, ease of processing, high mechanical and corrosion protection characteristics [2,5]. Different deposition techniques, such as hot-dip, galvanizing, and thermal spraying, are commonly used to provide good quality hard films [6,7]. The performance of such coatings is still quite sensitive to various environments that limit their utility [8]. Among the various coating techniques, electrodeposition is considered a simple and effective technique for metal deposition and has gained a lot of acceptance on a global scale [9,10].

The pulse electrodeposition (PE-deposition) is a unique coating technology that has recently gained substantial attention for the development of a range of alloy and composite coatings [11,12]. In the PE-deposition process, the current is supplied in pulses with equivalent amplitudes, intervals, and polarity that are separated through a zero-current value. In these sequences of pulses, each pulse is comprised of an ON-time (t_{on}), when current is supplied and an OFF-time (t_{off}), when no current is supplied to the circuit [13]. This mechanism provides the reverse current flow, which can eliminate the burr on the coating surface, resulting in an effective reduction in cathode concentration, improves the current density and decreases the occurrence of hydrogen embrittlement, and eliminates the use of additives which effectively save production costs [14]. The PE-deposition process gives some

* Corresponding authors.
E-mail addresses: shakoor@qu.edu.qa (R.A. Shakoor), bakr@qu.edu.qa (A.M. Abdullah), umer.adeel@scme.nust.edu.pk (M.A. Umer).
[1] Authors with equal contributions (Mostafa H. Sliem and Khuram Shahzad).

https://doi.org/10.1016/j.surfcoat.2020.126340
Received 13 June 2020; Received in revised form 11 August 2020; Accepted 20 August 2020
Available online 27 August 2020

prominent advantages such as ease of tailoring coating composition, ease of processing, controlling thickness in an atomic order, control of crystal structure, efficiency, and low cost. More importantly, the evolution of fine-grained coating structure results in improved mechanical and electrochemical properties. It is thus possible to synthesize various nanostructured coatings by modifying pulse parameters [15]. Despite the obvious advantages of PE-deposition, its potential has not been fully explored yet for the development of novel nickel-based composite coatings.

Currently, nickel-phosphorus coatings have attained high considerations due to their remarkable properties [16], demonstrating decent corrosion and wear resistance properties with good hardness [17]. However, their properties can further be enhanced by the incorporation of various types of reinforcements to address the industrial challenges [18]. Recent studies reveal that the addition of ceramic reinforcements improves the structural, mechanical, and corrosion protection properties of nickel-based coatings. Many types of reinforcements have been studied so far including diamond [19], BN [20], Al_2O_3 [21], TiO_2 [22], Cr_2N [23], graphene oxide [24], duplex W-ZrO_2 [25], CeO_2-RuO_2 [26], CNT [27], SiC [28], PTFE [29], Gr-SiC [30], Si_3N_4 [31], SiO_2 [32], and B_4C [33]. Here, it is also worth mentioning that the development of coatings made by the incorporation of these reinforcements has mainly been achieved through the electroless or simple electrodeposition techniques. The PE-deposition method has not been fully investigated for the synthesis of a lot of composite coatings, although some reports are available in literature [34–36].

This study is primarily dedicated to exploring the possible fabrication and characteristics of NiP-ZrO_2 coatings through the PE-deposition technique. The effects of concentration of ZrO_2 nanoparticles (ZONPs) on surface morphology, mechanical, microstructure, and corrosion protection properties of NiP coatings have been examined by employing various characterization techniques to elucidate the useful role of ZONPs in the NiP matrix. The novelty of the study exists in the fact that the synthesis and in-depth analysis of PE-deposited NiP-ZrO_2 nanocomposite (NC-coatings) have not been explored yet. In fact, most of the previously published works on NiP-ZrO_2 coatings are based on either electroless or the simple electrodeposition process [37,38].

2. Experimental details

2.1. Materials

For the development of NiP and NiP-ZrO_2 NC-coatings through PE-deposition process, an electrolyte bath which was composed of analytical grade nickel sulphate hexahydrate ($NiSO_4{\cdot}6H_2O$, as a source of nickel), nickel chloride hexahydrate ($NiCl{\cdot}6H_2O$), sodium chloride (NaCl), sodium hypophosphite (NaH_2PO_2, as a source of phosphorus), boric acid (H_3BO_3), and phosphoric acid (H_3PO_4). High purity zirconium dioxide nanoparticles (ZONPs) with an average particle size < 50.0 nm were used as nanoparticle reinforcement. All chemicals were purchased from Sigma Aldrich. Pulse electrodeposition of NiP and NiP-ZrO_2 NC-coatings was carried out on low alloy steel (30CrMnSi, Chinse grade) substrate, which was purchased from Wugang Chang Yu Long Industry And Trade Co., Ltd., China. The substrate samples have dimensions of 30 × 30 × 2 mm^3 with an elemental composition, as shown in Table 1.

Table 1
The elemental composition of the 30CrMnSi steel sheet.

Element	C	Si	Mn	Ni	Cr	S & P	Balance
wt.%	0.28	1.2	0.9	0.3	1.1	0.025	Fe

Table 2
Chemical composition and operating conditions for the PE-deposition coating bath.

Sr. no	Chemical name	Composition
1	Nickel sulphate hexahydrate (g/L)	250
2	Nickel chloride hexahydrate (g/L)	30
3	Sodium chloride (g/L)	15
4	Boric acid (g/L)	30
5	Phosphoric acid (g/L)	6
6	Sodium hypophosphite (g/L)	20
7	ZrO_2 nanoparticles (ZONPs) (g/L)	(0.0, 0.25, 0.50, 0.75, & 1.0) g/L)
Operating conditions		
8	pH	2.5 ± 0.1
9	Temperature	50 °C
10	Magnetic stirrer (Bath agitation)	300 rpm
11	Deposition time	999 s
12	Current density	10 A/dm^2
13	Frequency	100 Hz
14	Duty Cycle %	50
15	t (t_{on} + t_{off})	10 s
16	t_{on}	5 s
17	t_{off}	5 s

2.2. Deposition process

The substrate samples were ground and polished successively with various grit sized SiC abrasive papers (220, 320, 500, 800, 1000, 1200 up to 2000) to achieve the flat and smooth surfaces. Polished samples were then degreased by sonicating for 15 min in acetone, followed by washing with warm distilled water. One side of the substrates was masked, enabling electrodeposition only on a single surface. The uncovered surface was activated using a 20% H_2SO_4 solution for 30 s. In the end, the activated substrates were thoroughly washed with hot water and were directly immersed in the electrolyte bath to start the deposition process under the conditions composed in Table 2. The electrolyte bath was continuously agitated with a magnetic stirrer at 300 rpm to keep ZONPs in suspension during the deposition process. Further, to reduce ZONPs agglomeration, ultrasonic sonication was undertaken for 30 min before the commencement of the deposition process [39–41]. After deposition processing, the coated samples were removed, rinsed, and dried. This procedure was repeated for each concentration of ZONPs to obtain the different NC-coatings compositions. The developed NiP-ZrO_2 NC-coatings were designated as per the ZONPs concentrations, which were dispersed into the electrolyte bath. In this perspective, the obtained coatings samples were labeled as NiP, NiP-0.25ZrO_2, NiP-0.5ZrO_2, NiP-0.75ZrO_2, and NiP-1.0 ZrO_2, respectively. For a clear understanding, a schematic diagram of the PE-deposition process used during the current work is shown in Fig. 1.

2.3. Characterization

FE-SEM (field emission scanning electron microscope) from Nova, Nano-450, Netherland, equipped with EDX (energy-dispersive X-ray spectroscopy), and AFM (atomic force microscope) from Asylum Research, Oxford Instruments, Goleta, USA, were utilized to explore the morphological, compositional and surface characteristics of the prepared NC-coatings. The structural and phase analysis was determined using the X-rays diffractometer (from Rigaku, Miniflex2 Desktop, Tokyo, Japan), equipped with Cu Kα radiations). The diffraction patterns were recorded at a scan step size of 0.02°/s in the 2θ range from 20° to 60°. The chemical composition of the prepared NC-coatings was also analyzed with X-ray photoelectron spectroscopy (XPS) using Kratos Axis Ultra DLD X-ray spectrometer, UK, with employing a monochromatic Al-Kα X-rays source; the binding energy of C 1s (284.6 eV) was utilized as a reference for calibration. The full survey was maintained at 160 eV passing energy, and the high-resolution spectra were taken place at 20 eV passing energy. Microhardness of the developed coatings

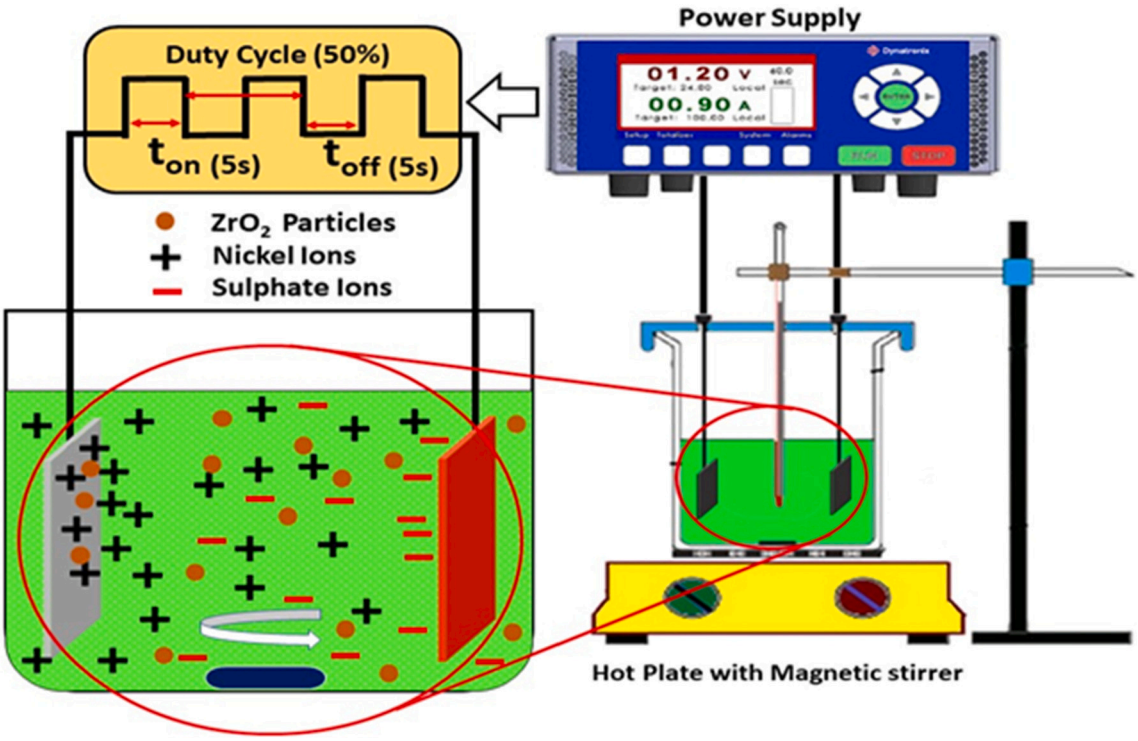

Fig. 1. Schematic diagram of the PE-deposition process for the synthesis of NiP and NiP-ZrO_2 NC-coatings.

was evaluated using FM-ARS9000 Vickers microhardness tester (USA). All microhardness tests were performed under 100 gf loading, providing a holding time of 10 s at the peak load. The presented results are an average of five readings. Nanoindentation was carried out using the MFP-3D nanoindenter head connected to AFM. The nanoindentation tests were performed with Berkovich diamond indenter tip using a maximum 1mN indentation force. The mechanical values were determined from the load vs. displacement curve using the Oliver-Pharr method.

The corrosion protection properties of the prepared coatings containing were investigated in a brine solution (3.5 wt% NaCl) at room temperature. All electrochemical measurement was performed through a three-electrode system using a GAMRY 3000 potentiostat (Gamry, Warminster, PA, USA). All specimens were placed in OCP (open-circuit potential) conditions for 30 min before staring electrochemical measurements. Electrochemical Impedance Spectroscopy (EIS) was performed with an amplitude of 10 mV (AC) versus OCP at frequency range 100,000–0.01 Hz. Moreover, the potentiodynamic polarization study was conducted at −250 mV to +250 mV versus OCP, applying a scan rate of 0.167 mV s^{-1}. Additionally, all tests were repeated three times to ensure reproducibility.

3. Results and discussion

3.1. Surface morphology

The surface morphology of as-prepared NiP and NiP-ZrO_2 NC-coatings containing different concentrations of ZONPs was studied using FESEM, and the results are presented in Fig. 2(a–e). The formation of a compact structure is evident in all the coatings. Fig. 2(a) corresponds to NiP coatings, which depicts a relatively smooth surface containing some spherical nodules. A comparison of the micrographs of NiP-ZrO_2 NC-coatings presented in Fig. 2(b–e) indicates that NiP-ZrO_2 NC-coatings have more nodular structure as compared to the pure NiP coatings. Moreover, the size of the nodules decreases with an increasing amount of ZONPs into the NiP matrix Fig. 2(b–e). This reduction in nodular size leads to the formation of a more dense and compact coating structure, which is expected to improve the structural, mechanical, and corrosion protection properties [42]. Fig. 3 depicts the formation mechanism of NiP NC-coatings upon adding ZNOPs into the Ni—P bath solution. It suggests that the addition of ZONPs has a substantial effect on the morphology of NiP coatings. A gradual increase in the amount of ZONPs into the coating bath during the PE-deposition process leads to their progressive incorporation into the NiP matrix, which ultimately affects the evolution of finer nodules and compact grains. The reduction in grain size and the formation of more nodules can also be regarded as the effect of the process of heterogeneous nucleation. Incremental addition of ZONPs into the NiP matrix may also lead to accelerating the nucleation rate providing more nucleation sites and thus reduces the lateral growth of the grains, which ultimately results in smaller nodules [43]. Moreover, the porosity of the coatings may also be reduced with increasing concentration of ZONPs into the NiP matrix due to: (i) grain refinement which leads to the formation of compact structure and (ii) filling of pores by the ZONPS which block the pore openings and contributing in making the structure of the coating more compact [44]. Further, to have more details on the topographic features of the NiP alloy and NiP-ZrO_2 coatings containing various concentrations of ZONPs, AFM study was undertaken. The 3D images, along with roughness profiles of NiP alloys and NiP-ZrO_2 NC-coatings, are shown in Fig. 4(a–e). A comparison of AFM images and roughness profiles indicates that the addition of ZONPs has a pronounced effect on surface profile, topography, and roughness of NiP-ZrO_2 NC-coatings. NiP coatings have relatively smooth surfaces; however, the surface of NiP-ZrO_2 NC-coatings composed of small hills and valleys. The average surface-roughness of the NiP alloy coatings increases with the increasing amount of ZONPs. The results show that the surface roughness of the NiP coatings is 4.374 nm, which gradually increases with an increasing amount of ZONPs reaching to 16.706 nm at the terminal composition 1.0 g/L ZONPs. This increase in surface roughness can be attributed to the existence of hard and insoluble ZONPs in the NiP alloy matrix. These results are also consistent with the previous studies [5,45].

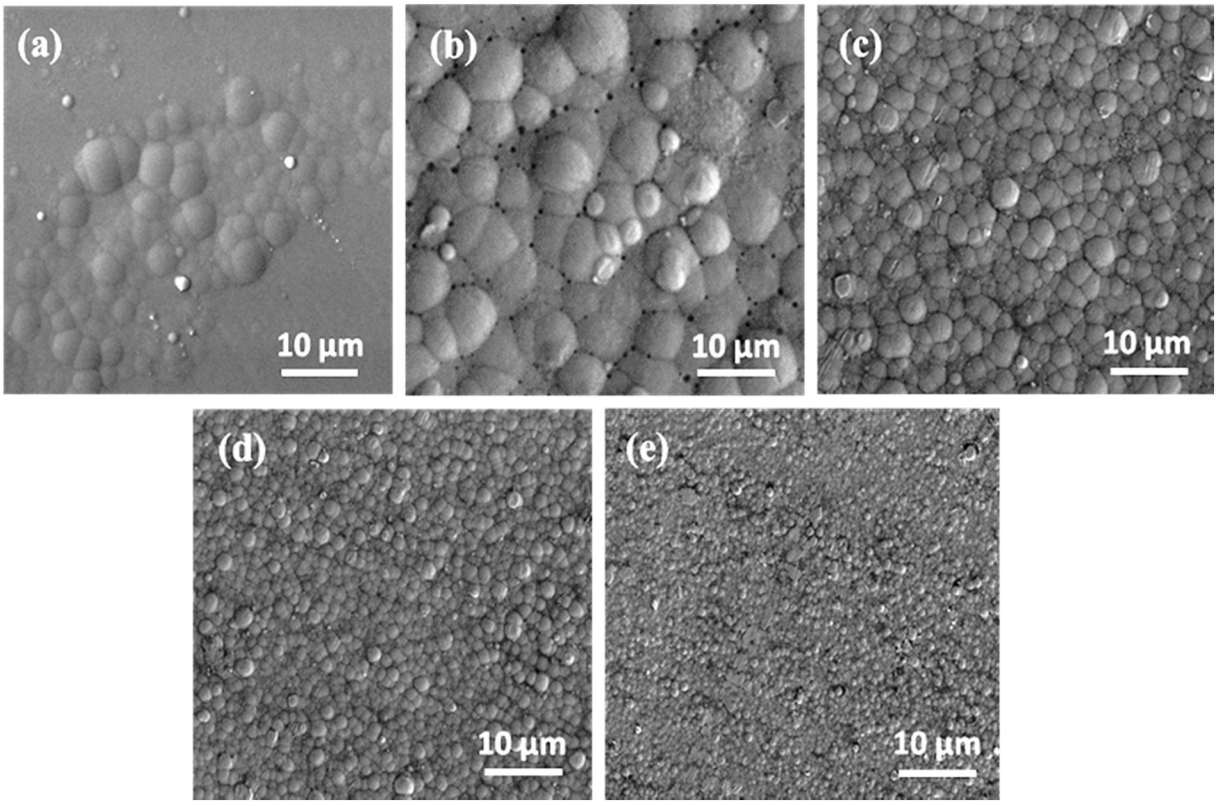

Fig. 2. FE-SEM micrographs of the NiP and NiP-ZrO_2 NC-coatings that contains various concentration of ZONPs (a) 0.0, (b) 0.25, (c) 0.50, (d) 0.75, and (e) 1.0 g/L.

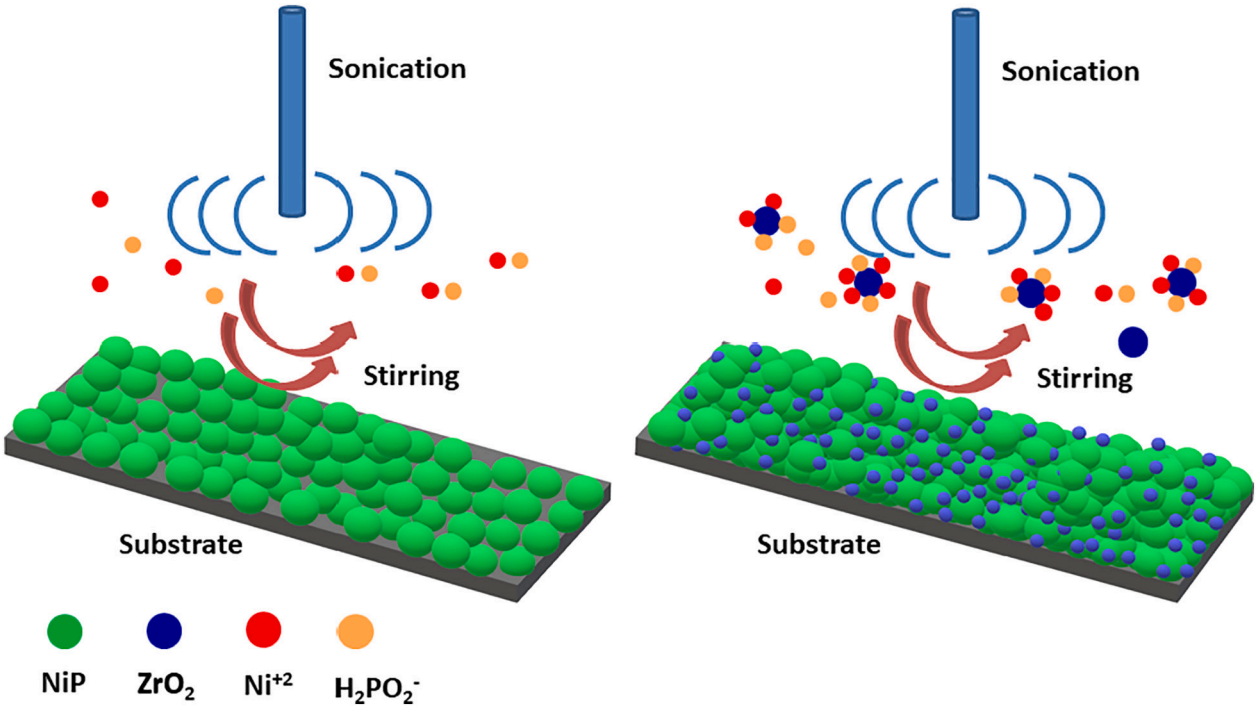

Fig. 3. Schematic diagram for the deposition mechanism of the NiP-NC-coatings.

3.2. Structural and composition analysis

3.2.1. XRD study

Fig. 5(a) depicts the XRD patterns of the as-deposited NiP and NiP-ZrO_2 NC-coatings containing various contents of ZONPs (0.0, 0.25, 0.50, and 1.0 g/L). All XRD spectra show a predominated broad peak at 2θ of 44.5, representing the face-centered cubic structure of Ni (111) with amorphous like structure. However, the diffraction peak of Ni (111) shows a strong intensity peak accompany the broad one which indicating a semi-crystalline structure of the developed coatings in their as-plated condition. Similar results have been reported in the literature due to two factors: (i) the presence of phosphorus atoms in the crystal

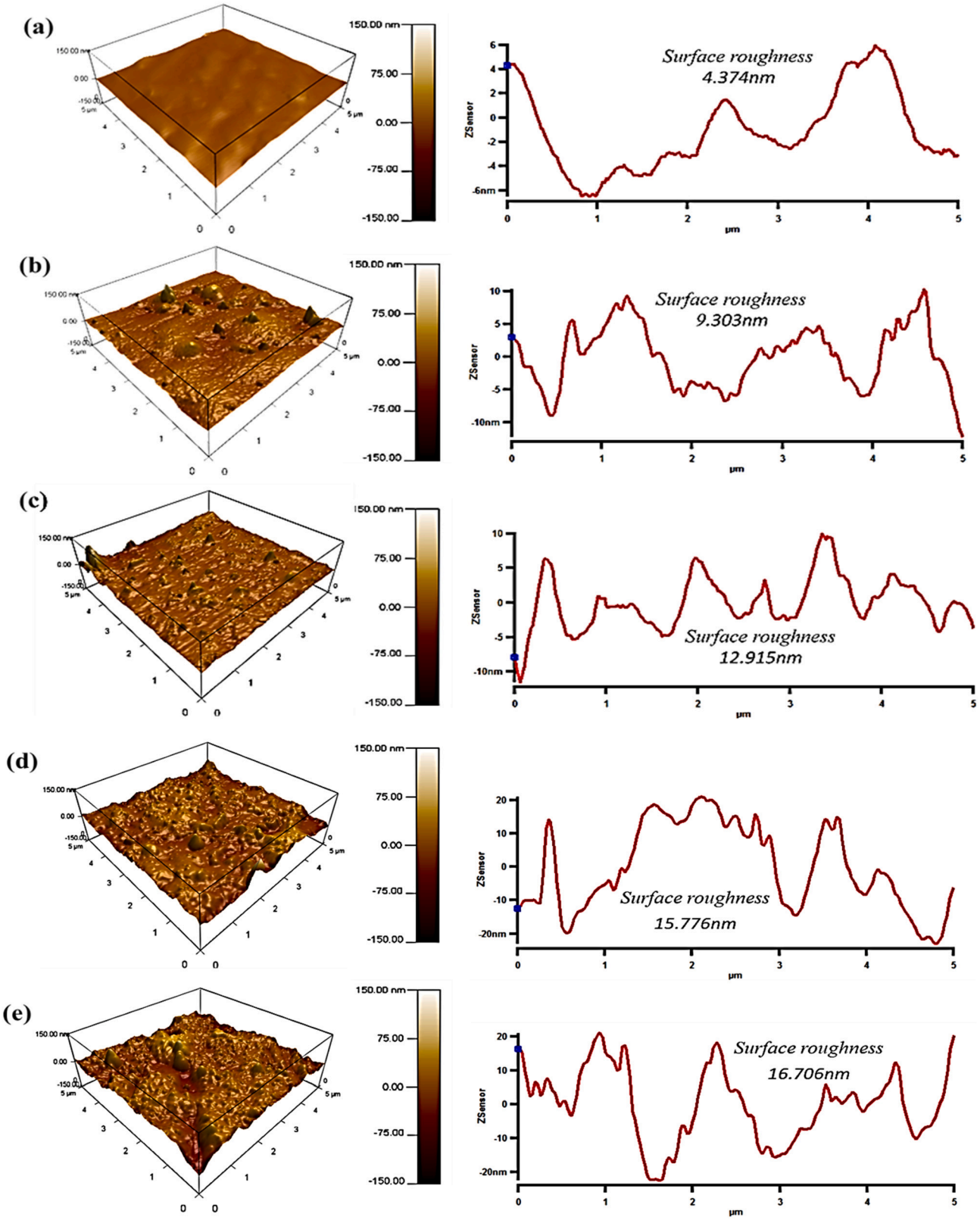

Fig. 4. 3D-AFM topographic images along with respective surface-roughness profiles of (a) NiP (b) NiP-0.25ZrO_2, (c) NiP-0.5ZrO_2, (d) NiP-0.75ZrO_2, and (e) NiP-1.0ZrO_2 coatings.

lattice of nickel which can change the columnar structure to fibrous grains, and their coalescence leads to the lattice distortion [46], and (ii) the heterogeneous nucleation process due to the incorporation of ZONPs during the development of the coating [47–51]. A magnified view of the XRD pattern is also shown in Fig. 5 (b). The presence of low-intensity peaks located at 2θ of 28.2 and 31.5 shows the presence of ZONPs into the NiP matrix. An increase in the intensity of peaks of $ZrO_2(-111)$ and $ZrO_2(111)$ with increasing concentration of ZONPs is

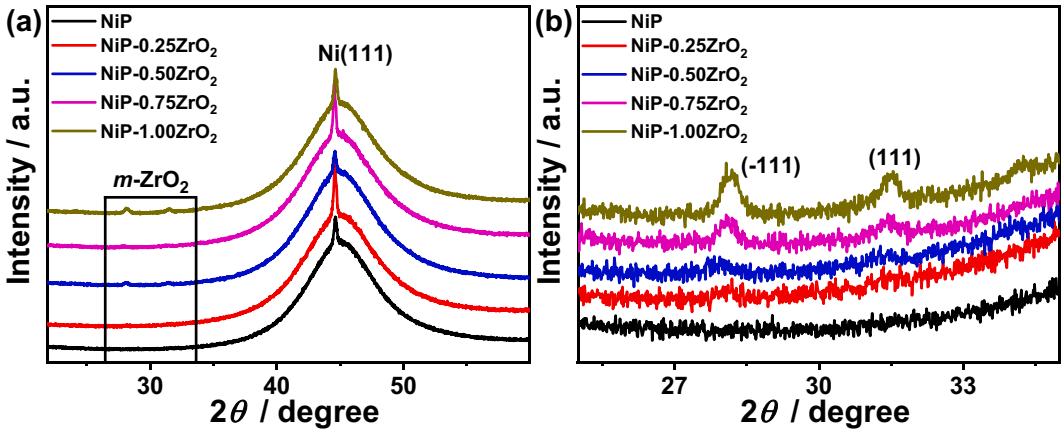

Fig. 5. XRD pattern for NiP and NiP-ZrO_2 NC-composite coatings containing various concentrations of ZONPs (0.25, 0.5, 0.75, and 1.0 g/L).

noticed, indicating incremental co-deposition of ZONPs into the NiP matrix. The low intensity of $ZrO_2(-111)$ and $ZrO_2(111)$ can be attributed to the inherent high intensity of nickel peaks and the low quantity of ZONPs in the NiP matrix. A similar trend for some other reinforcements has also been reported in the literature [44,52].

3.2.2. X-ray photoelectron spectroscopy (XPS) analysis

The X-ray photoelectron spectroscopy (XPS) analysis was performed to depict the compositional alteration in the NiP matrix due to the incorporation of ZONPs. Fig. 6 illustrates the survey spectrum of NiP and NiP-ZrO_2 NC-coatings containing only 1.0 g/L ZONPs. The elemental peaks of Ni 2p, P 2p, O 1s, C 1s, Fe 2p in the NiP coatings indicates that these coatings are composed of Ni, P, C, O, and Fe elements. Whereas, the presence of additional bands of Zr 3d along with Ni 2p, P 2p, O 1s, C 1s, Fe 2p in the NiP-ZrO_2 NC-coatings confirms the incorporation of ZONPs into the NiP matrix. The C 1s band comes from the surface as an impurity. The O 1s band comes not only from ZrO_2 nanoparticles but also from the coating surface as an impurity [53]. The Fe 2p bands are essentially originated from the steel substrate. The high-energy resolution spectrum for Ni 2p, P 2p, and Zr 3d signals of NiP and NiP-1.0 ZrO_2 NC-coatings are presented in Fig. 7(a, c) and (b, d & e) respectively. Furthermore, the position of the recorded peaks and the full width at half of the maximum were tabulated in Table 3. It can be noticed that the Ni 2p spectra can be nominated into two main dominated peaks of Ni $2p_{3/2}$ at 853.4 eV and a peak of Ni $2p_{1/2}$ at 869.8 eV, respectively Fig. 7(a & b), which are corresponding to the metallic nickel. Additionally, the satellite peaks of Ni $2p_{3/2}$ at 858.4 eV and Ni $2p_{1/2}$ at 874.8 eV are associated with $Ni^{+2,}$ which would be representative of NiO or $Ni(OH)_2$ [44,54]. Intriguingly, the predominant and satellite peaks for Ni 2p is shifted by 0.5 eV towards the higher binding energy value from its nominal position after adding 1.0 g/L ZONPs Fig. 7(b). Moreover, the satellite peaks show a significant increase in its intensity, which attributed to increasing the formation of oxide and hydroxide phases [55]. The P 2p spectra in Fig. 7(c & d) can be consisted of four peaks corresponding to 129.2 eV, 129.9 eV, 131.2 eV and 133.4 eV. The peaks positioned at 129.2 eV and 129.9 eV are assigned to the P (phosphorus) as P $2p_{1/2}$ and to the NiP alloy, respectively, as the phosphorous signal intensity diminished with the Ni combination. Furthermore, the central peak at the binding energy of 131.2 eV could be ascribed to the first or the third valence state of phosphorus, which could be originated from the residual hypophosphite. Additionally, the peak located at 133.4 eV possibly be attributed to a mixture of POx chemical states for instance (P_2O_3 and P-OH), which could be notified at the binding energy close to 134.5 [55,56]. Fig. 7(e) depicts the high-resolution spectrum of Zr 3d as it assures the presence of two signals at 182.3 eV and 184.8 eV, which assigned to Zr $3d_{5/2}$ and Zr-$3d_{1/2}$, respectively which confirms the existence of ZONPs into the NiP-ZrO_2 NC-coatings.

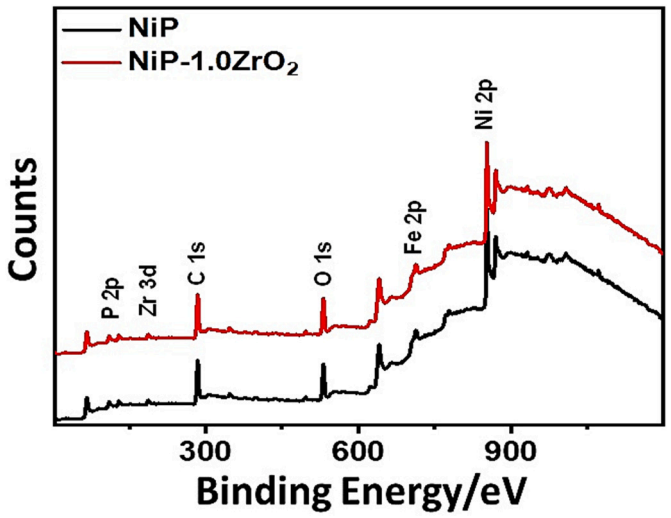

Fig. 6. XPS wide-scan survey spectrum for NiP and NiP-1.0 ZrO_2 NC-coatings.

3.2.3. Energy-dispersive X-ray spectroscopy (EDX) analysis

The co-deposition of ZONPs into the NiP alloy matrix was also analyzed by the EDX technique, and the results are shown in Fig. 8(a–e). For clarity purposes, the quantitative compositional analysis of NiP and each NiP-ZrO_2 NC-coatings are also shown as an inset in each EDX graph. The EDX analysis confirms the presence of ZONPs in the NiP matrix. It can be further noticed that the co-deposition of ZONPs is accomplished at the cost of both nickel (Ni) and phosphorus (P), as evident by the reduction in the Ni and P contents with the increasing amount of ZONPs into the NiP matrix. These results show that the developed NiP and NiP-ZrO_2 NC-coatings containing various concentrations of ZONPs can be classified into high phosphorus coatings. It is due to the fact that NiP coatings are having phosphorous contents > 9.0 wt% are usually classified as high phosphorous coatings [57]. Moreover, the thickness of the NC-coating was duplicated from ~7 μm for the plain NiP coating to ~15 μm for NiP-1.0 ZrO_2 NC-coating, as presented in Fig. 9. It can be evidenced that the presence of the ZrO_2 in the matrix promotes the deposition process with good adherence. In the meantime, there is a uniform distribution of ZrO_2 in the coating layer. Furthermore, it can also be revealed that the NiP-ZrO_2 nc-coatings is composed of the compact structure without any defect at the interface of the substrate and coating.

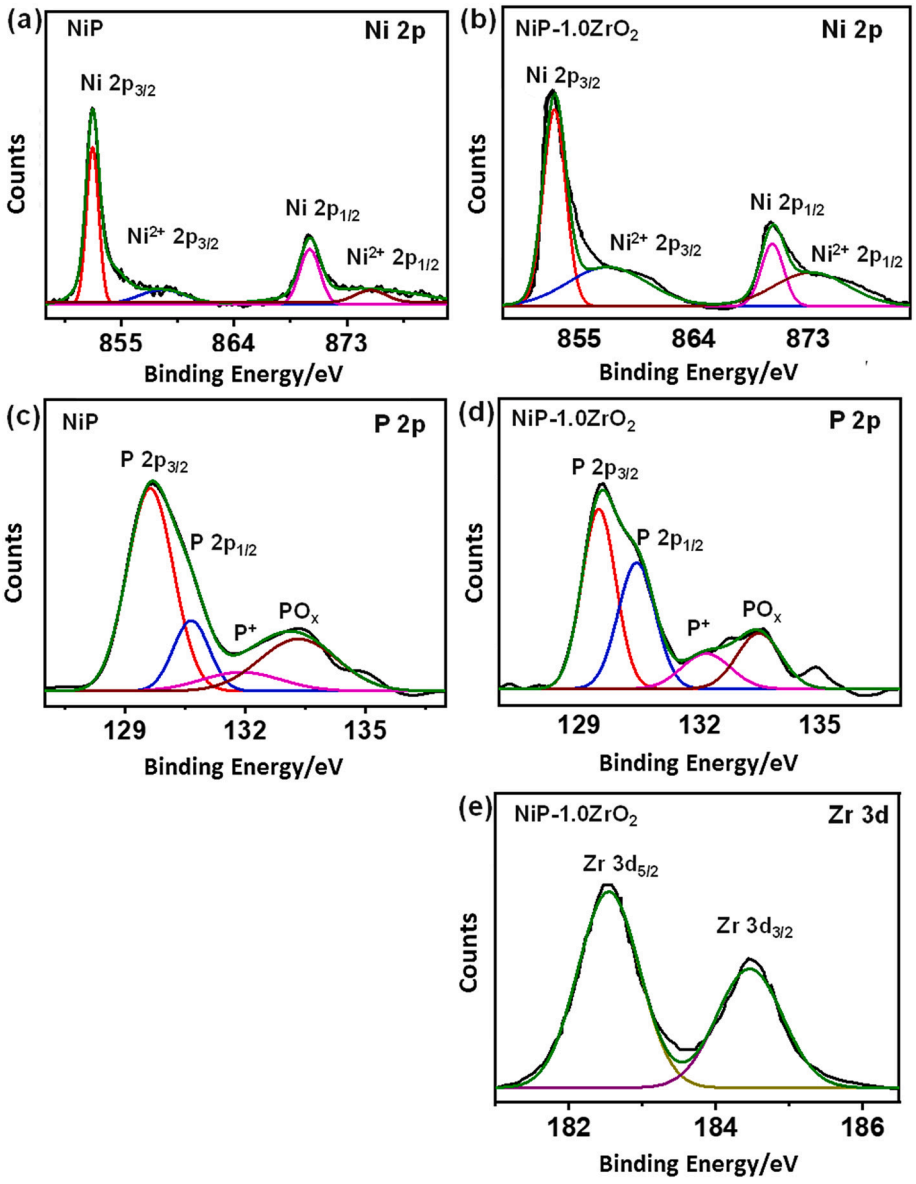

Fig. 7. High-energy resolution spectrum for Ni-2p, P-2p, and Zr-3d signals of NiP and NiP-1.0ZrO_2 NC-coatings.

Table 3
Binding energy and FWHM of the main elements in NiP and NiP-1.00ZrO_2 NC-coatings.

Coating	Element	Peak	Position	FWHM
NiP	Ni	Ni $2p_{3/2}$	852.1	1.29
		Ni^{2+} $2p_{3/2}$	858.4	5.69
		Ni $2p_{1/2}$	869.8	2.11
		Ni^{2+} $2p_{1/2}$	875.1	7.22
	P	$2p_{1/2}$	129.1	1.25
		$2p_{1/2}$	129.7	1.24
		P^+	131.2	0.93
		PO_x	133.4	2.44
NiP-1.00ZrO_2	Ni	Ni $2p_{3/2}$	852.1	2.09
		Ni^{2+} $2p_{3/2}$	858.4	7.33
		Ni $2p_{1/2}$	869.8	2.07
		Ni^{2+} $2p_{1/2}$	875.1	6.78
	P	$2p_{1/2}$	129.1	0.99
		$2p_{1/2}$	129.7	1.09
		P^+	131.2	1.43
		PO_x	133.4	1.28
	Zr	$3d_{5/2}$	182.5	0.98
		$3d_{3/2}$	184.7	1.05

3.3. Mechanical performance

The mechanical properties of NiP and NiP-ZrO_2 NC-coatings containing various concentrations of ZONPs were evaluated through microhardness and nanoindentation techniques. Fig. 10(a) shows the microhardness results of NiP and NiP-ZrO_2 NC-coatings containing different contents of ZONPs. The microhardness of binary NiP coatings is around ~540 HV_{100}. In contrast, the supplemental addition of ZONPs into the NiP alloy matrix leads to the gradual increase in the microhardness, which reaches to ~667 HV_{100} at the terminal composition 1.0 g/L ZONPs. The increase in the microhardness values of the NiP-ZrO_2 NC-coatings seems to vary linearly with the ZONPs in the matrix. The improvement in the microhardness of the NiP alloy by adding ZONPs can be attributed to the dispersion hardening effect and grain refinement [11,45]. In dispersion hardening, it is presumed that the precipitates (nanoparticles) do not deform with the matrix, and the moving dislocations have to bypass the obstacles provided by the ZONPs by changing the deformation path between precipitates [58], whereas in the grain refinement process, a grain refiner can act as a heterogeneous nucleation site during the solidification [59]. In our case, ZONPs dispersed into the deposition bath may provide various

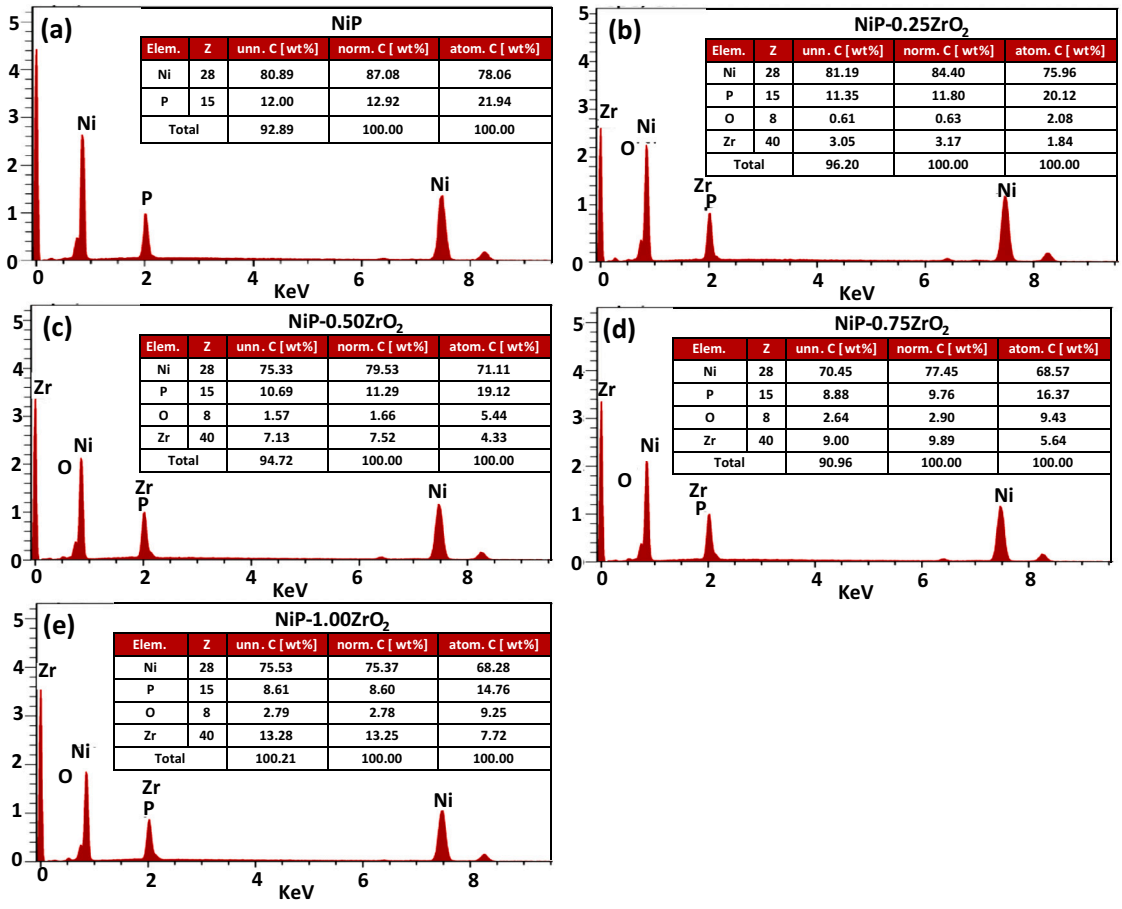

Fig. 8. EDX composition analysis of: (a) NiP and (b, c. d, e) NiP-ZrO_2 NC coatings with various concentrations of ZNOPs (0.25, 0.5, 0.75, and 1.0 g/L).

heterogeneous nucleation sites leading to accelerating the nucleation rate, which reduces the lateral growth of the grains and thus ultimately forms a fine-grained structure. The strengthening mechanism through grain refinement can also be expressed by the Hall-Petch equation as described below [60]:

$$\sigma_y = \sigma_0 + kd^{-1/2} \quad (1)$$

$$HV \approx 3\sigma_y \quad (2)$$

where σ_y is the yield stress and σ_0 is a material stress constant required to start dislocation motion, k is a constant, d is the diameter of grain, and HV is microhardness. The decrease in grain size with the increasing amount of ZONPs can also be clearly seen in the FE-SEM images Fig. 2(a–e).

A comparison of load vs. displacement curves representing the nanomechanical behavior of NiP and NiP-ZrO_2 NC-coatings is presented in Fig. 10(b). A decrease in indentation depth at constant loading with the increasing amount of ZONPs is observed, which confirms the increase in the hardness of NiP-ZrO_2 NC-coatings. The hardness of the binary NiP coatings is 5.3GPa, which gradually increases with an increasing amount of ZONPs in the NiP matrix. The highest value of hardness (6.7GPa) is achieved at the terminal composition of NiP-1.0 ZrO_2,

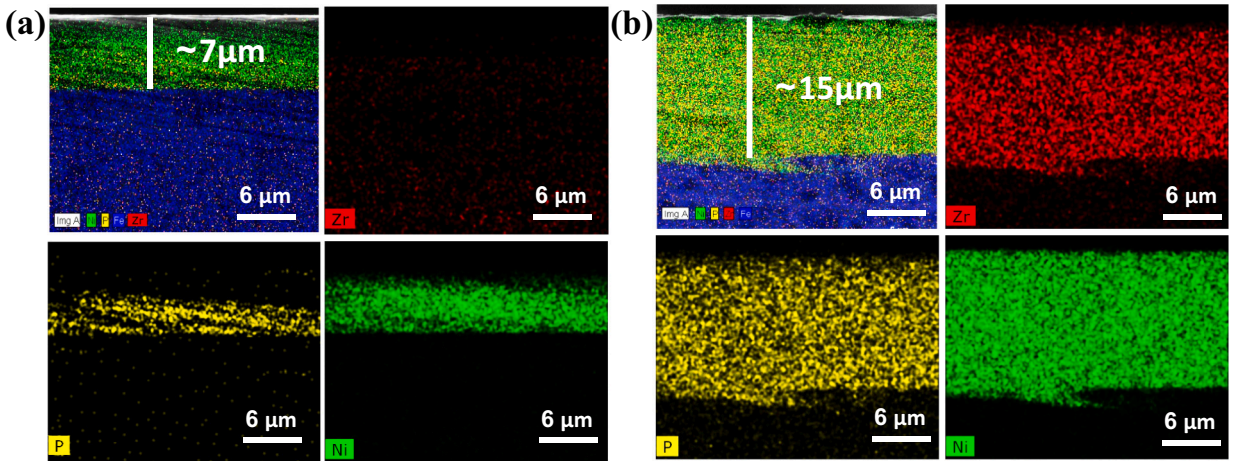

Fig. 9. Elemental mapping analysis at the cross-section of NiP and NiP-1.0ZrO_2 NC- coatings.

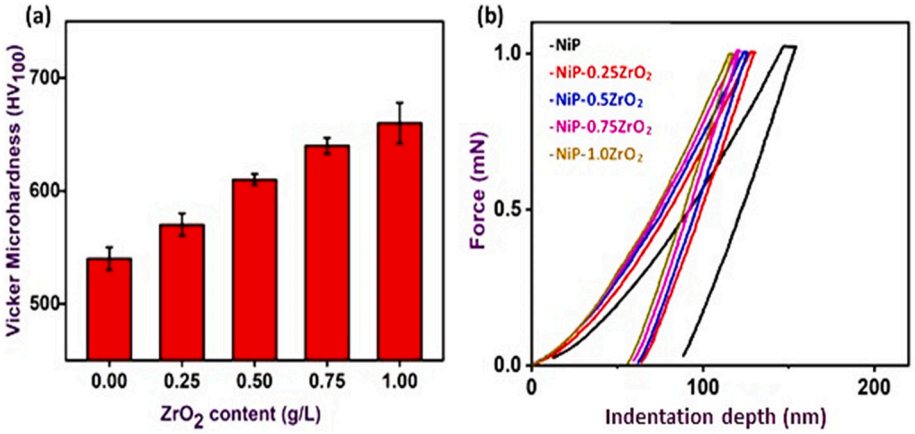

Fig. 10. Mechanical properties of NiP and NiP-ZrO_2 NC-coatings; (a) Vickers microhardness and (b) nanoindentation load-displacement curves.

depicting an improvement of ~30% when compared to binary NiP alloy coatings. Similarly, the modulus of NiP coating is ~11.17 GPa for which increases with the increasing concentrations of ZONPs and attains its maximum value of 21.72 GPa at the terminal composition. This increase in mechanical properties of the coatings can also be attributed to the formation of a composite structure along with the dispersion hardening and grain refinement effects [61]. The contribution of the formation of a composite structure in improving the properties of NiP-ZrO_2 NC-coatings can be calculated following the rule of the mixture [62].

$$E_c = E_m V_m + E_p V_P \tag{3}$$

where E stands for modulus, V for the volume fraction, c for composite, m for matrix, and p for particulates, to sum up, it can be deduced that the improvement in the mechanical properties of NiP-ZrO_2 NC-coatings with an increasing amount of ZONPs can be ascribed to three factors: (i) dispersion hardening, (ii) grain refinement and (iii) formation of a composite structure [45,62,63].

3.4. Corrosion protection properties

3.4.1. Electrochemical Impedance Spectroscopy (EIS)

The electrochemical impedance spectra of NiP and NiP-ZrO_2 NC-coatings with varying amounts of ZONPs were recorded in 3.5 wt% NaCl solution to investigate the corrosion protective properties, and the results are presented in Fig. 11(a & b). The EIS spectra were fitted using the equivalent circuit having two-time constant depicted in Fig. 11(c), and the calculated parameters are presented in Table 4. The equivalent circuit consists of (R_s), which is assigned to the resistance of solution, R_1 shows the pore-resistance, and R_2 represents the charge transfer resistance of the metallic coating, respectively, whereas *CPE*1 and *CPE*2 are constant phase elements for their opponent resistances. The *CPE* is mainly used as a substitution for the regular capacitor element owing to the surface roughness or the coating heterogeneity, which is attributed to the irregular thickness of the as-deposited coatings. The impedance values can be deducted by using the following equation [64]:

$$Z_{CPE} = \frac{1}{Q(i\omega)^n} \tag{4}$$

where Q is a function of the general admittance ($s^n\,\Omega^{-1}\,cm^{-2}$), ω is the frequency of the AC signal (rad/s), n is the deviation of the ideal capacitance from the real capacitance as the n value approach to the unity. The value of charge transfer resistance (R_2) increases continuously with the increasing amount of ZONPs in the NiP matrix.

Furthermore, the concentration of ZONPs plays a crucial role in enhancing the coating barrier properties as it can be seen that the values of pore resistance (R_1) gradually increases with the increasing amount of ZONPs into the NiP matrix and reaches to 1824 $\Omega\,cm^{-2}$ at the terminal composition which is 9-fold higher than the binary NiP coatings (284 $\Omega\,cm^{-2}$). Additionally, the admittance values of the *CPE* between the electrolyte and coating also reduces with the increase of concentration of ZONPs into the NiP matrix, as seen in Fig. 11(d). This improvement in the corrosion protection behavior of NiP coatings by the addition of ZONPs can be ascribed primarily to factors such as (i) reduction in the active area of the NiP alloy matrix due to the presence ceramic ZONPs, (ii) filling or blocking of pores by the ZONPs, and (iii) double-layer capacitances which decreased due to the presence ZNOPs that restrict of the Cl^- ions to reach the metal surface [65]. Fig. 12 demonstrates the open circuit potential and the potentiodynamic polarization behavior of the NiP and NiP-ZrO_2 NC-coatings containing different concentrations of ZONPs. The steady-state potential for the as-synthesized NC-coatings can be achieved after 25 min of exposure in the aggressive media, and increasing the ZONPs contents shift the OCP value to the Nobel direction as seen in Fig. 12(a). Additionally, it can be noted that the polarization curves are shifted to the less negative potential and the lower current densities with the increasing amount of ZONPs into the NiP matrix, as shown in Fig. 12(b). For a clear comparison, the electrochemical corrosion parameters derived from potentiodynamic polarization curves, such as corrosion potential (E_{corr}), corrosion current density (i_{corr}), cathodic and anodic Tafel extrapolation (βc and βc, respectively), and polarization resistance (R_p) are also tabulated in Table 5. The corrosion current density of each sample was determined by manipulating Tafel extrapolation. The polarization resistance (R_p) was determined using the Stern-Geary equation, as seen below [66]:

$$R_p = \frac{\beta_a * \beta_c}{2.303 * i_{corr} * (\beta_a + \beta_c)} \tag{5}$$

It can also be noted that the obtained R_p values from the potentiodynamic polarization technique are compatible with the values of EIS test [67]. Additionally, the values of cathodic and anodic current densities decrease with an increasing amount of ZONPs into the NiP alloy matrix. The i_{corr} value (27.4 $\mu A\,cm^{-2}$) of the binary NiP alloys coating is the highest among all the prepared coatings, which decreases with increasing concentration of ZONPs into the NiP matrix and reaches to its lowest value of 2.21 $\mu A\,cm^{-2}$ at the terminal composition. Moreover, comparing the corrosion current densities of the developed coatings with that of bare carbon steel, which was reported in the authors' previous publication, reveals that pulse electrodeposited NiP-ZrO_2 NC-coatings are more favorable to be utilized in the saline environments [68]. As discussed earlier, the enhanced corrosion resistance of the NiP alloy matrix due to the incorporation of ZONPs can be observed as the effect of reduction in the active area of the NiP matrix due to the existence of inactive ceramic particles [65].

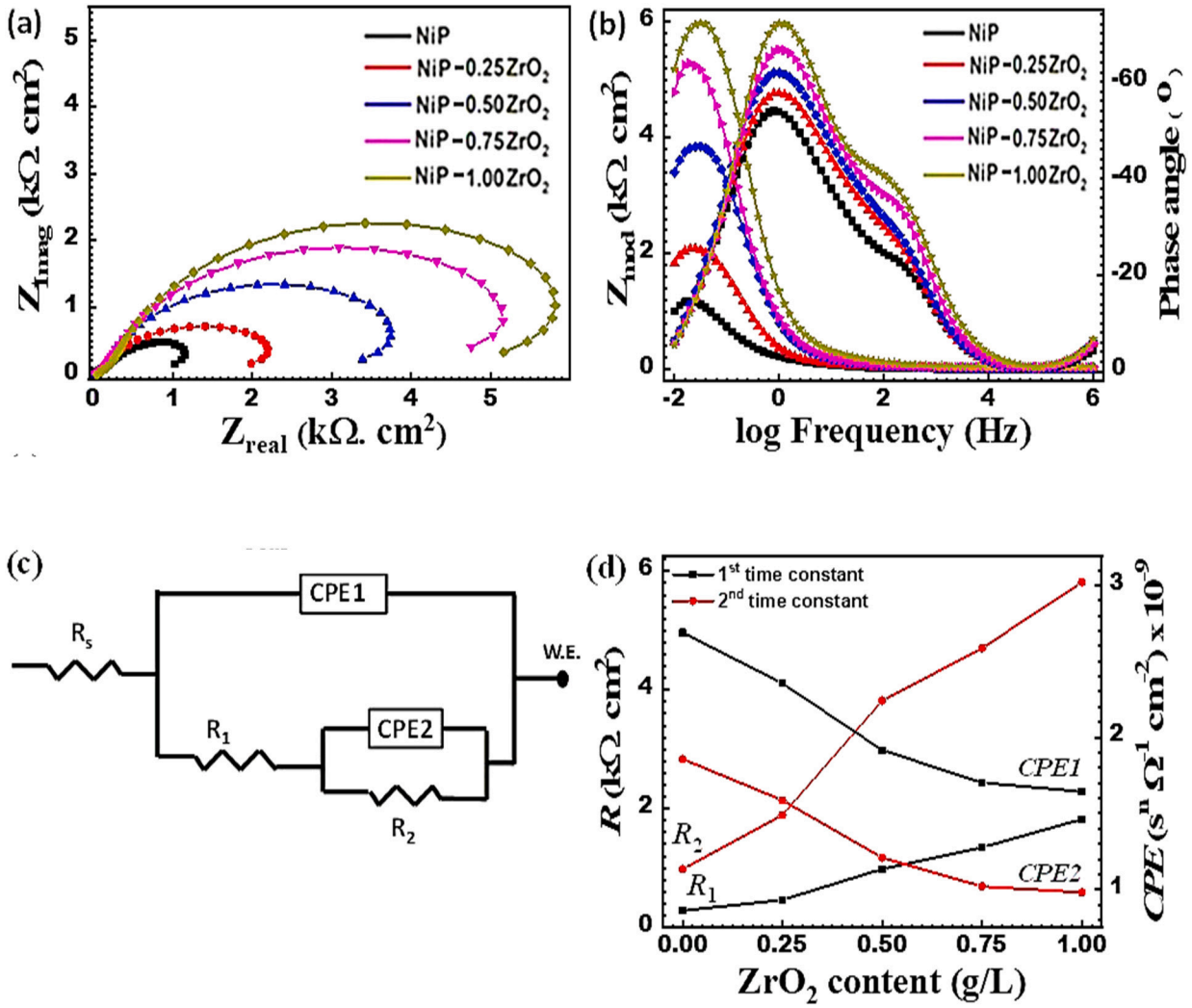

Fig. 11. EIS analysis of NiP and NiP-ZrO_2 NC-coatings; (a) Nyquist plot, (b) Bode and phase angle diagram, (c) the equivalent circuit for impedance spectrum analysis and (d) impedance capacitance curves versus ZNOPs content in NiP-ZrO_2 NC-coatings.

4. Conclusions

NiP-ZrO_2 nanocomposite coatings containing various concentrations of ZrO_2 nanoparticles (ZONPs) were successfully deposited on low alloy steel (30CrMnSi) substrate through the pulse electrodeposition technique. The structural and compositional analyses confirm the formation of phase pure coatings and the successful co-deposition of ZONPs into the NiP matrix. The addition of ZONPs has a significant influence on the structural, mechanical, and corrosion protection properties of NiP coatings. A gradual improvement in the mechanical properties of NiP coatings is noticed with the addition of ZONPs into the matrix that reaches to its ultimate value for NiP-1.0 ZrO_2 composition (hardness 6.7 GPa, modulus 21.72 GPa). Similarly, the corrosion protection efficiency of the NiP coatings increases with an increasing amount of ZONPs reaching an eventual value ~5.8 kΩ cm^{-2} at NiP-1.0 ZrO_2 composition, which is six times higher than the pure NiP coatings. A comparative analysis of the developed coatings concludes that NiP-1.0 ZrO_2 nanocomposite coatings demonstrate superior mechanical and corrosion protection properties and thus can be considered for their potential applications in the oil and gas pipeline.

CRediT authorship contribution statement

Mostafa H. Sliem: Conceptualization, Investigation, Data curation, Writing - review & editing. **Khuram Shahzad:** Data curation, Methodology, Writing - review & editing. **V.N. Sivaprasad:** Investigation, Data curation. **R.A. Shakoor:** Conceptualization, Supervision, Writing - review & editing. **Aboubakr M. Abdullah:**

Table 4
EIS parameters for NiP and NiP-ZrO_2 NC-coatings (containing various content of ZNOPs, 0.25, 0.5, 0.75 and 1.0 g/L) immersed in 3.5 wt% NaCl solution.

Sample	R_s Ω cm^2	R_1 Ω cm^2	$CPE1 \times 10^{-6}$ $s^n \Omega^{-1} cm^{-2}$	n_1	R_2 Ω cm^2	$CPE2 \times 10^{-6}$ $s^n \Omega^{-1} cm^{-2}$	n_2
NiP	7.49	283.1	2689	0.71	982.6	1857	0.84
NiP-0.25ZrO_2	7.62	464.5	2355	0.91	1894	1586	0.67
NiP-050ZrO_2	7.75	983.7	1916	0.76	3821	1208	0.86
NiP-0.75 ZrO_2	7.92	1349	1702	0.73	4703	1020	0.77
NiP-1.00ZrO_2	7.58	1824	1643	0.72	5817	980.1	0.84

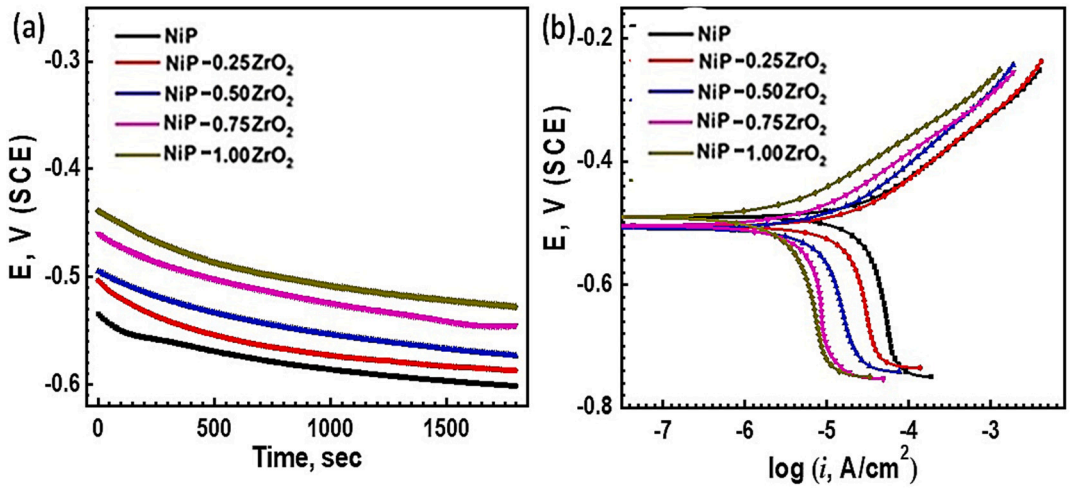

Fig. 12. (a) Open circuit potential and (b) potentiodynamic polarization curves of NiP and NiP-ZrO_2 NC-coatings containing various concentrations of ZONPs (0.25, 0.5, 0.75, and 1.0 g/L) in 3.5 wt% NaCl medium.

Table 5
Electrochemical corrosion parameters determined from potentiodynamic polarization curves of the NiP and NiP-ZrO_2 NC-coatings (containing various concentrations of ZONPs) immersed in 3.5 wt.% NaCl medium.

Sample	E_{corr} (mV) SCE	β_a (mV dec.$^{-1}$)	β_c (mV dec.$^{-1}$)	$i_{corr,}$ (μA cm^{-2})	R_p Ω cm^2
NiP	−491.2	110.7	115.6	27.4	897.31
NiP-0.25ZrO_2	−506.1	128.1	125.9	15.7	1758.3
NiP-050ZrO_2	−509.0	178.8	133.6	12.0	2770.4
NiP-0.75 ZrO_2	−505.2	134.7	120.5	6.24	4431.6
NiP-1.00ZrO_2	−409.0	112.03	73.2	2.21	8709.9

Conceptualization, Supervision, Writing - review & editing. **Osama Fayyaz:** Methodology, Data curation. **Ramazan Kahraman:** Investigation, Data curation. **Malik Adeel Umer:** Conceptualization, Supervision, Writing - review & editing.

Declaration of competing interest

The authors declare that they have no known competing financial interests or personal relationships that could have appeared to influence the work reported in this paper.

Acknowledgment

This publication was made possible by QU Grant, IRCC-2020-006. Statements made herein are solely the responsibility of the authors. The microstructural analysis (FE-SEM/EDX) was accomplished at the Central Laboratory Unit (CLU), Qatar University (QU), Doha, Qatar.

References

[1] H.K. Karapanagioti, H. Takada, Hazardous Chemicals Associated with Plastics in the Marine Environment, (2019), https://doi.org/10.1007/698.
[2] A. Popoola, O. Olorunniwo, O. Ige, Corrosion resistance through the application of anti-corrosion coatings, Dev. Corros. Prot. (2014), https://doi.org/10.5772/57420.
[3] M. Mozetič, Surface modification to improve properties of materials, Materials (Basel) 12 (2019) 441, https://doi.org/10.3390/ma12030441.
[4] J. Prakash, B.M. Tripathi, S.K. Ghosh, Low Temperature Coating Deriving from Metal-Organic Precursors: An Economical and Environmentally Benign Approach, Elsevier Inc., 2015, https://doi.org/10.1016/B978-0-12-411467-8.00004-0.
[5] K.M. Zadeh, R.A. Shakoor, A. Bahgat Radwan, Structural and electrochemical properties of electrodeposited Ni-P nanocomposite coatings containing mixed ceramic oxide particles, Int. J. Electrochem. Sci. 11 (2016) 7020–7030, https://doi.org/10.20964/2016.08.42.
[6] B. Jodoin, L. Ajdelsztajn, E. Sansoucy, A. Zúñiga, P. Richer, E.J. Lavernia, Effect of particle size, morphology, and hardness on cold gas dynamic sprayed aluminum alloy coatings, Surf. Coat. Technol. 201 (2006) 3422–3429, https://doi.org/10.1016/j.surfcoat.2006.07.232.
[7] S. Matthews, B. James, Review of thermal spray coating applications in the steel industry: part 2 — zinc pot hardware in the continuous galvanizing line, J. Therm. Spray Technol. 19 (2010) 1277–1286, https://doi.org/10.1007/s11666-010-9519-7.
[8] B. Fotovvati, N. Namdari, A. Dehghanghadikolaei, On coating techniques for surface protection: a review, J. Manuf. Mater. Process. 3 (2019) 28, https://doi.org/10.3390/jmmp3010028.
[9] F.G. Arieta, D.T. Gawne, The wettability and durability of chromium plating, Surf. Coat. Technol. 73 (1995) 105–110, https://doi.org/10.1016/0257-8972(94)02371-9.
[10] K.M. Yin, C.M. Wang, A study on the deposit uniformity of hard chromium plating on the interior of small-diameter tubes, Surf. Coat. Technol. 114 (1999) 213–223, https://doi.org/10.1016/S0257-8972(99)00046-8.
[11] K. Saber, C.C. Koch, P.S. Fedkiw, Pulse current electrodeposition of nanocrystalline zinc, Mater. Sci. Eng. A 341 (2003) 174–181, https://doi.org/10.1016/S0921-5093(02)00198-3.
[12] I. Bakonyi, W.E.G. Hansal, Development of pulse-plating technology for the preparation of coatings with varying composition along their thickness: a historical overview, Trans. Inst. Met. Finish. 96 (2018) 237–243, https://doi.org/10.1080/00202967.2018.1503853.
[13] S. Roy, Electrodeposition of compositionally modulated alloys by a electrodeposition-displacement reaction method, Surf. Coat. Technol. 105 (1998) 202–205, https://doi.org/10.1016/S0257-8972(98)00455-1.
[14] N.S. Qu, D. Zhu, K.C. Chan, W.N. Lei, Pulse electrodeposition of nanocrystalline nickel using ultra narrow pulse width and high peak current density, Surf. Coat. Technol. 168 (2003) 123–128, https://doi.org/10.1016/S0257-8972(03)00014-8.
[15] S. Ahmadiyeh, A. Rasooli, M.G. Hosseini, Ni–B/SiC nanocomposite coating obtained by pulse plating and evaluation of its electrochemistry and mechanical properties, Surf. Eng. 35 (2019) 861–872, https://doi.org/10.1080/02670844.2018.1498823.
[16] A. Lelevic, Ni-P coatings electroplating — a review, part I: pure Ni-P alloy, http://arxiv.org/abs/1807.04693, (2018).
[17] E.C. Kedward, K.W. Wright, A.A.B. Tennett, The development of electrodeposited composites for use as wear control coatings on aero engines, Tribology 7 (1974) 221–227, https://doi.org/10.1016/0041-2678(74)90120-1.
[18] C.S. Ramesh, R. Keshavamurthy, B.H. Channabasappa, A. Ahmed, Microstructure and mechanical properties of Ni-P coated Si_3N_4 reinforced Al6061 composites, Mater. Sci. Eng. A 502 (2009) 99–106, https://doi.org/10.1016/j.msea.2008.10.012.
[19] X. Xi, R. Zhang, F. Sun, Effect of phosphorus content on suspension of Ni-P coated diamond (NPCD) and wear resistance of electrodeposited Ni-Co-Mn/NPCD composite coatings, Diam. Relat. Mater. 74 (2017) 164–172, https://doi.org/10.1016/j.diamond.2017.03.010.
[20] C.I. Hsu, K.H. Hou, M. Der Ger, G.L. Wang, The effect of incorporated self-lubricated BN(h) particles on the tribological properties of Ni-P/BN(h) composite coatings, Appl. Surf. Sci. 357 ((2015) 1727–1735, https://doi.org/10.1016/j.apsusc.2015.09.207.
[21] S. Afroukhteh, C. Dehghanian, M. Emamy, Preparation of electroless Ni–P composite coatings containing nano-scattered alumina in presence of polymeric surfactant, Prog. Nat. Sci. Mater. Int. 22 (2012) 318–325, https://doi.org/10.1016/j.pnsc.2012.06.006.
[22] Y. Wang, W. Chen, A. Shakoor, R. Kahraman, W. Lu, B. Yan, W. Gao, Ni-P-TiO_2 composite coatings on copper produced by sol-enhanced electroplating, Int. J. Electrochem. Sci. 9 (2014) 4384–4393.
[23] D. Kong, X. Zuo, Y. Wang, Y. Zhou, Microstructure and thermal decomposition property of Ni-P/Cr2N composite powder by electroless plating, Adv. Powder Technol. 29 (2018) 1433–1438, https://doi.org/10.1016/j.apt.2018.03.005.

[24] H. Wu, F. Liu, W. Gong, F. Ye, L. Hao, J. Jiang, S. Han, Preparation of Ni-P-GO composite coatings and its mechanical properties, Surf. Coat. Technol. 272 (2015) 25–32, https://doi.org/10.1016/j.surfcoat.2015.04.028.

[25] H. Luo, M. Leitch, H. Zeng, J.L. Luo, Characterization of microstructure and properties of electroless duplex Ni-W-P/Ni-P nano-ZrO_2 composite coating, Mater. Today Phys. 4 (2018) 36–42, https://doi.org/10.1016/j.mtphys.2018.03.001.

[26] S.M.A. Shibli, A.H. Riyas, M. Ameen Sha, R. Mole, Tuning of phosphorus content and electrocatalytic character of CeO_2-RuO_2 composite incorporated Ni-P coating for hydrogen evolution reaction, J. Alloys Compd. 696 (2017) 595–603, https://doi.org/10.1016/j.jallcom.2016.11.238.

[27] A. Zarebidaki, S.R. Allahkaram, Effect of surfactant on the fabrication and characterization of Ni-P-CNT composite coatings, J. Alloys Compd. 509 (2011) 1836–1840, https://doi.org/10.1016/j.jallcom.2010.10.057.

[28] M. Franco, W. Sha, V. Tan, S. Malinov, Insight of the interface of electroless Ni-P/SiC composite coating on aluminium alloy, LM24, Mater. Des. 85 (2015) 248–255, https://doi.org/10.1016/j.matdes.2015.06.159.

[29] Q. Zhao, Y. Liu, Electroless Ni-Cu-P-PTFE composite coatings and their anticorrosion properties, Surf. Coat. Technol. 200 (2005) 2510–2514, https://doi.org/10.1016/j.surfcoat.2004.06.011.

[30] M.F. He, W. Bin Hu, C. Zhong, J.F. Weng, B. Shen, Y.T. Wu, Effect of wear conditions on tribological properties of electrolessly-deposited Ni-P-Gr-SiC hybrid composite coating, Trans. Nonferrous Met. Soc. China (English Ed.) 22 (2012) 2586–2592, https://doi.org/10.1016/S1003-6326(11)61504-5.

[31] U. Matik, Structural and wear properties of heat-treated electroless Ni-P alloy and Ni-P-Si_3N_4 composite coatings on iron based PM compacts, Surf. Coat. Technol. 302 (2016) 528–534, https://doi.org/10.1016/j.surfcoat.2016.06.054.

[32] A. Sadeghzadeh-Attar, G. AyubiKia, M. Ehteshamzadeh, Improvement in tribological behavior of novel sol-enhanced electroless Ni-P-SiO_2 nanocomposite coatings, Surf. Coat. Technol. 307 (2016) 837–848, https://doi.org/10.1016/j.surfcoat.2016.10.026.

[33] M. Ebrahimian-Hosseinabadi, K. Azari-Dorcheh, S.M.M. Vaghefi, Wear behavior of electroless Ni-P-B4C composite coatings, Wear. 260 (2006) 123–127, https://doi.org/10.1016/j.wear.2005.01.020.

[34] A. Zoikis-Karathanasis, E.A. Pavlatou, N. Spyrellis, Pulse electrodeposition of Ni-P matrix composite coatings reinforced by SiC particles, J. Alloys Compd. 494 (2010) 396–403, https://doi.org/10.1016/j.jallcom.2010.01.057.

[35] K.H. Hou, Y.C. Chen, Preparation and wear resistance of pulse electrodeposited Ni-W/Al_2O_3 composite coatings, Appl. Surf. Sci. 257 (2011) 6340–6346, https://doi.org/10.1016/j.apsusc.2011.01.089.

[36] F. Xia, H. Xu, C. Liu, J. Wang, J. Ding, C. Ma, Microstructures of Ni-AlN composite coatings prepared by pulse electrodeposition technology, Appl. Surf. Sci. 271 (2013) 7–11, https://doi.org/10.1016/j.apsusc.2012.12.064.

[37] B. Szczygieł, A. Turkiewicz, J. Serafińczuk, Surface morphology and structure of Ni-P, Ni-P-ZrO_2, Ni-W-P, Ni-W-P-ZrO_2 coatings deposited by electroless method, Surf. Coat. Technol. 202 (2008) 1904–1910, https://doi.org/10.1016/j.surfcoat.2007.08.016.

[38] F. Hou, W. Wang, H. Guo, Effect of the dispersibility of ZrO_2 nanoparticles in Ni-ZrO_2 electroplated nanocomposite coatings on the mechanical properties of nanocomposite coatings, Appl. Surf. Sci. 252 (2006) 3812–3817, https://doi.org/10.1016/j.apsusc.2005.05.076.

[39] I. Tudela, Y. Zhang, M. Pal, I. Kerr, A.J. Cobley, Ultrasound-assisted electrodeposition of composite coatings with particles, Surf. Coat. Technol. 259 (2014) 363–373, https://doi.org/10.1016/j.surfcoat.2014.06.023.

[40] M.C. Chou, M. Der Ger, S.T. Ke, Y.R. Huang, S.T. Wu, The Ni-P-SiC composite produced by electro-codeposition, Mater. Chem. Phys. 92 (2005) 146–151, https://doi.org/10.1016/j.matchemphys.2005.01.021.

[41] Y.F. Tian, X.H. Li, Z.H. Ao, Y.J. Xue, Corrosion resistance of Ni-ZrO_2 nanocomposite coating prepared by pulse electrodeposition with rotating cathode in an ultrasonic field, Appl. Mech. Mater. 278–280 (2013) 422–425, https://doi.org/10.4028/www.scientific.net/AMM.278-280.422.

[42] R. Hu, Y. Su, Y. Liu, H. Liu, Y. Chen, C. Cao, H. Ni, Deposition process and properties of electroless Ni-P-Al_2O_3 composite coatings on magnesium alloy, Nanoscale Res. Lett. 13 (2018) 2–9, https://doi.org/10.1186/s11671-018-2608-0.

[43] B. Bakhit, A. Akbari, Synthesis and characterization of Ni-Co/SiC nanocomposite coatings using sediment co-deposition technique, J. Alloys Compd. 560 (2013) 92–104, https://doi.org/10.1016/j.jallcom.2013.01.122.

[44] 43-Properties enhancement of Ni-P electrodeposited coatings by the Ni-P-Y_2O_3.pdf, (n.d.).

[45] R.A. Shakoor, A. Bahgat Radwan, Remarkable improvement in properties of NI-B coatings by the addition of mixed oxide nanoparticles, Mater. Sci. Technol. Conf. Exhib. 2015, MS T 2015. 1, 2015, pp. 171–178.

[46] W. Sha, X. Wu, K.G. Keong, Crystallisation of nickel–phosphorus (Ni–P) deposits with high phosphorus content, Electroless Copp. Nickel–Phosphor. Plat. (2011) 141–162, https://doi.org/10.1533/9780857090966.2.141.

[47] J.N. Balaraju, T.S.N. Sankara Narayanan, S.K. Seshadri, Structure and phase transformation behaviour of electroless Ni-P composite coatings, Mater. Res. Bull. 41 (2006) 847–860, https://doi.org/10.1016/j.materresbull.2005.09.024.

[48] M. Czagány, P. Baumli, G. Kaptay, The influence of the phosphorous content and heat treatment on the nano-micro-structure, thickness and micro-hardness of electroless Ni-P coatings on steel, Appl. Surf. Sci. 423 (2017) 160–169, https://doi.org/10.1016/j.apsusc.2017.06.168.

[49] J.P. Randin, Chemical nature of phosphorus in Ni—P deposits, J. Appl. Phys. 43 (1972) 4834–4835, https://doi.org/10.1063/1.1661032.

[50] P.H. Lo, W.T. Tsai, J.T. Lee, M.P. Hung, Role of phosphorus in the electrochemical behavior of electroless Ni-P alloys in 3.5 wt.% NaCl solutions, Surf. Coat. Technol. 67 (1994) 27–34, https://doi.org/10.1016/S0257-8972(05)80023-4.

[51] W.Y. Chen, H.W. Chen, W.P. Li, J.C. Huang, H.S. Yu, J.G. Duh, S. Lan, T. Feng, Compositionally modulated microstructure in nano-layered Ni-P metallic glass composite coating prepared by electrodeposition, Surf. Coat. Technol. 389 (2020), https://doi.org/10.1016/j.surfcoat.2020.125636.

[52] H.H. Sheu, S.Y. Jian, M.H. Lin, C.I. Hsu, K.H. Hou, M. Der Ger, Electroless Ni-P/PTFE self-lubricating composite thin films applied for medium-carbon steel substrate, Int. J. Electrochem. Sci. 12 (2017) 5464–5482, https://doi.org/10.20964/2017.06.30.

[53] P. Tao, M. Mei-Hua, X. Fei-Bo, X. Xin-Quan, XPS and AES investigation of nanometer composite coatings of Ni-P-ZnX on steel surface (ZnX = $ZnSnO_3$, $Zn_3(PO_4)_2$, $ZnSiO_3$), Appl. Surf. Sci. 181 (2001) 191–195, https://doi.org/10.1016/S0169-4332(01)00343-9.

[54] M.C. Biesinger, B.P. Payne, L.W.M. Lau, A. Gerson, R.S.C. Smart, X-ray photoelectron spectroscopic chemical state quantification of mixed nickel metal, oxide and hydroxide systems, Surf. Interface Anal. 41 (2009) 324–332, https://doi.org/10.1002/sia.3026.

[55] Z. Qi, W. Lee, XPS study of CMP mechanisms of NiP coating for hard disk drive substrates, Tribol. Int. 43 (2010) 810–814, https://doi.org/10.1016/j.triboint.2009.11.007.

[56] B. Elsener, D. Atzei, A. Krolikowski, V.R. Albertini, C. Sadun, R. Caminiti, A. Rossi, From Chemical to Structural Order of Electrodeposited, (2004), pp. 4216–4225.

[57] R. Taheri, I.N.A. Oguocha, S. Yannacopoulos, The tribological characteristics of electroless NiP coatings, Wear 249 (2001) 389–396, https://doi.org/10.1016/S0043-1648(01)00539-7.

[58] R.E. Smallman, A.H.W. Ngan, R.E. Smallman, A.H.W. Ngan, Chapter 13 – precipitation hardening, Mod. Phys. Metall. (2014) 499–527, https://doi.org/10.1016/B978-0-08-098204-5.00013-4.

[59] W. Li, J. Mao, J. Feng, Aluminium grain refinement by Ti(C, N) nanoparticles additions: principles, advantages and drawbacks, Metall. Res. Technol. 116 (2019), https://doi.org/10.1051/metal/2018083.

[60] Y. Song, J. Yeon, B. Na, Numerical simulations of the hall-petch relationship in aluminium using gradient-enhanced plasticity model, Adv. Civ. Eng. 2019 (2019), https://doi.org/10.1155/2019/7356581.

[61] V. Torabinejad, M. Aliofkhazraei, A.S. Rouhaghdam, M.H. Allahyarzadeh, T. Kasama, H. Alimadadi, Mechanical properties of multilayer Ni-Fe and Ni-Fe-Al_2O_3 nanocomposite coating, Mater. Sci. Eng. A 700 (2017) 448–456, https://doi.org/10.1016/j.msea.2017.06.009.

[62] H.S. Kim, On the rule of mixtures for the hardness of particle reinforced composites, Mater. Sci. Eng. A 289 (2000) 30–33, https://doi.org/10.1016/S0921-5093(00)00909-6.

[63] H.S. Kim, S.I. Hong, S.J. Kim, On the rule of mixtures for predicting the mechanical properties of composites with homogeneously distributed soft and hard particles, J. Mater. Process. Technol. 112 (2001) 109–113, https://doi.org/10.1016/S0924-0136(01)00565-9.

[64] K. Shahzad, M.H. Sliem, R.A. Shakoor, A.B. Radwan, R. Kahraman, M.A. Umer, U. Manzoor, A.M. Abdullah, Electrochemical and thermodynamic study on the corrosion performance of API X120 steel in 3.5% NaCl solution, Sci. Rep. 10 (2020) 1–15, https://doi.org/10.1038/s41598-020-61139-3.

[65] A.B. Radwan, R.A. Shakoor, Aluminum nitride (AlN) reinforced electrodeposited Ni–B nanocomposite coatings, Ceram. Int. (2020) 0–1, https://doi.org/10.1016/j.ceramint.2019.12.261.

[66] A. Bahgat Radwan, M.H. Sliem, P.C. Okonkwo, M.F. Shibl, A.M. Abdullah, Corrosion inhibition of API X120 steel in a highly aggressive medium using stearamidopropyl dimethylamine, J. Mol. Liq. 236 (2017) 220–231, https://doi.org/10.1016/j.molliq.2017.03.116.

[67] W. Zhang, C. Ji, B. Li, Synthesis and properties of Ni–W/ZrO_2 nanocomposite coating fabricated by pulse electrodeposition, Results Phys 13 (2019) 102242, , https://doi.org/10.1016/j.rinp.2019.102242.

[68] A. Zoikis-Karathanasis, E.A. Pavlatou, N. Spyrellis, Pulse electrodeposition of Ni-P matrix composite coatings reinforced by SiC particles, J. Alloys Compd. 494 (2010) 396–403, https://doi.org/10.1016/j.jallcom.2010.01.057.